

Atomistic Simulation of Boron Nitride Nanotubes Under Bending



T. Nguyen-Van, T. Nguyen-Danh and Q. Le-Minh

Abstract We investigate the bending buckling behavior of boron nitride (BN) nanotubes through molecular dynamics finite element method with Tersoff potential. Effects of the tube length on the critical bending buckling angle and moment are examined for (5, 5) BN armchair and (9, 0) BN zigzag tubes, which exhibit approximately identical diameters. The buckling and fracture mechanisms of the tubes under bending are considered and discussed with respect to various tube length–diameter ratios $L/D = 10\text{--}40$. Simulation results will help to design and use BN nanotube-based nanocomposites and nanodevices.

Keywords Atomistic simulation bending · Boron nitride nanotube Buckling

1 Introduction

A boron nitride nanotube (BN-NT) can be geometrically formed by rolling up a hexagonal boron nitride (BN) layer or a carbon nanotube (CNT) [1] in which alternating B and N atoms entirely substitute for C atoms as shown in Fig. 1.

Various techniques have been used to synthesize BN-NTs, including arc-discharge, chemical vapor deposition, laser ablation, ball-milling methods (see,

T. Nguyen-Van · T. Nguyen-Danh · Q. Le-Minh (✉)

Department of Mechanics of Materials and Structures, School of Mechanical Engineering,
Hanoi University of Science and Technology, Hanoi, Vietnam
e-mail: quy.leminh@hust.edu.vn

T. Nguyen-Van
e-mail: shachootrang@gmail.com

T. Nguyen-Danh
e-mail: tuong.nguyendanh@hust.edu.vn

T. Nguyen-Van
Faculty of Mechanical Engineering, Thai Nguyen University of Technology, Thai Nguyen,
Vietnam

© Springer Nature Singapore Pte Ltd. 2018

H. Nguyen-Xuan et al. (eds.), *Proceedings of the International Conference on Advances in Computational Mechanics 2017*, Lecture Notes in Mechanical Engineering, https://doi.org/10.1007/978-981-10-7149-2_12

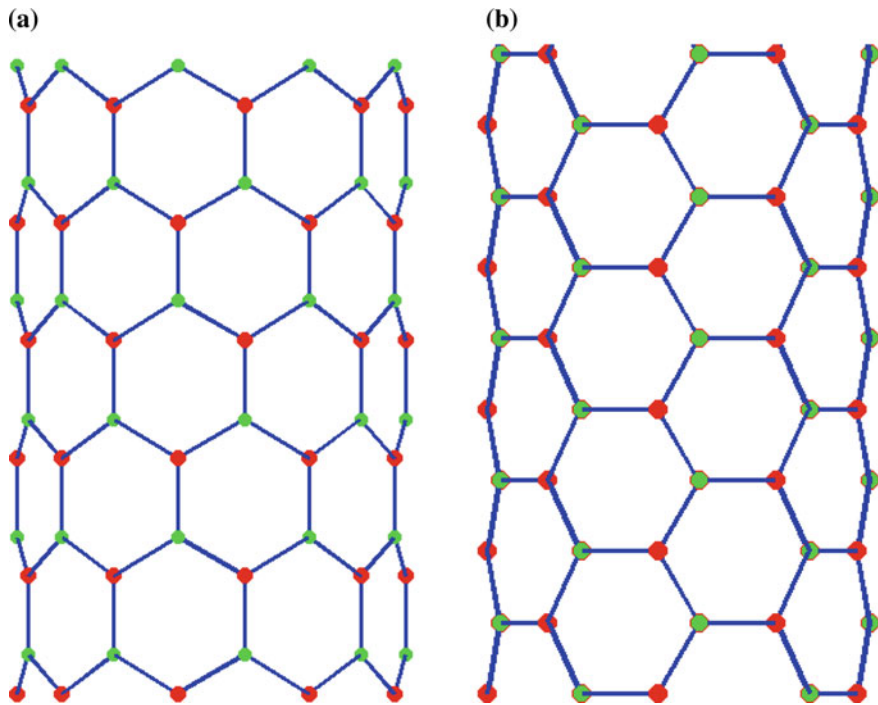


Fig. 1 Schematic illustration of: **a** (9, 0) BN zigzag tube; **b** (5, 5) BN armchair tube

e.g., the review by [2]). BN-NTs exhibit good mechanical properties with high elastic modulus of $\sim 0.5\text{--}1$ TPa and tensile strength of ~ 61 GPa [3]. They possess distinguishable chemical and thermal stability with high oxidation resistance up to 900°C in air [4], wide bandgaps independent of tube structures [5, 6], excellent thermal conductivity [7]. BN-NTs are also an effective violet and ultra-violet light emission material [8, 9]. Potential applications of BN-NTs include nanofillers in polymeric [10] and metallic [11] composites, optoelectronic fields [8], radiation shielding in space vehicles [12]. Potential applications of BN-NTs need a comprehension of the mechanical properties and performance of BN-NTs under various loading conditions. BN-NTs under compression [13–15], tension [16, 17], torsion [16, 18–20], and bending with two fixed or simple supports [21, 22] have been investigated. So far, theoretical studies of the buckling behavior under bending of BN-NTs seem unexplored. It should be noted that the buckling behavior of CNTs under bending has been investigated by continuum methods, atomistic simulations, and multi-scale approach; see, for example, [23, 24] and references therein.

The present work investigates through molecular dynamics finite element method (MDFEM) the buckling behavior of BN-NTs under bending. The critical bending buckling angle and moment are studied with respect to the length–diameter ratios of BN-NTs.

2 Framework for Analysis

Tersoff potential is used to model the B-N interatomic interactions [25]. The potential energy E of the atomic structure is a function of atomic coordinates as below:

$$E = \sum_i E_i = \frac{1}{2} \sum_{i \neq j} V_{ij}, V_{ij} = f_C(r_{ij}) [f_R(r_{ij}) + b_{ij} f_A(r_{ij})]; \quad (1a)$$

$$f_R(r_{ij}) = A_{ij} \exp(-\lambda_{ij}^I r_{ij}), f_A(r_{ij}) = -B_{ij} \exp(-\lambda_{ij}^H r_{ij}); \quad (1b)$$

$$f_C(r_{ij}) = \begin{cases} 1, & r_{ij} \leq R_{ij}; \\ \frac{1}{2} + \frac{1}{2} \cos\left(\pi \frac{r_{ij} - R_{ij}}{S_{ij} - R_{ij}}\right), & R_{ij} \leq r_{ij} \leq S_{ij}; \\ 0, & r_{ij} \geq S_{ij}; \end{cases} \quad (1c)$$

$$b_{ij} = \chi_{ij} \left(1 + \beta_i^{n_i} \zeta_{ij}^{n_i}\right)^{-1/2n_i}, \zeta_{ij} = \sum_{k \neq i,j} f_C(r_{ik}) \omega_{ik} g(\theta_{ijk}), g(\theta_{ijk}) \quad (1d)$$

$$= 1 + c_i^2/d_i^2 - c_i^2 / \left[d_i^2 + (h_i - \cos \theta_{ijk})^2\right]$$

$$\lambda_{ij}^I = (\lambda_i^I + \lambda_j^I)/2, \lambda_{ij}^H = (\lambda_i^H + \lambda_j^H)/2, A_{ij} = \sqrt{A_i A_j}, B_{ij} = \sqrt{B_i B_j}, R_{ij} \quad (1e)$$

$$= \sqrt{R_i R_j}, S_{ij} = \sqrt{S_i S_j}$$

Here, the lower indices i, j , and k label the atoms of the system, where interaction between atoms i and j is modified by a third atom k . r_{ij} is the distance between atoms i and j ; f_A and f_R are the attractive and repulsive pairwise terms; f_C is a cutoff function to ensure the nearest-neighbor interactions; R_{ij} and S_{ij} denote the small cutoff distance and the large one, respectively; b_{ij} is a bond-order parameter, depending on the local coordination of atoms around atom i . Further detail of the Tersoff potential is given in [25]. Force field parameters are taken from the work by Sevik et al. [26] for B-N interactions.

While the density functional theory (DFT) calculations and molecular dynamics (MD) simulations are time-consuming, molecular dynamic finite element methods (MDFEMs), sometimes known as atomic-scale finite element methods or atomistic finite element methods, have been developed to analyze nanostructured materials in a computationally efficient way; see, for example, [27, 28]. To achieve the atomic positions of the BN-NT under specific boundary conditions, molecular dynamic finite element method (MDFEM) is here adopted. In MDFEM, atoms and atomic displacements are considered as nodes and translational degrees of freedom (nodal displacements), respectively. Both first and second derivatives of system energy are used in the energy minimization computation, hence it is faster than the standard conjugate gradient method which uses only the first-order derivative of system energy as

discussed in [27]. The stiffness matrices of these elements are established based upon interatomic potentials. Similar to conventional finite element method, global stiffness matrix is assembled from element stiffness matrices. Hence, relations between atomic displacement and force can be derived by solving a system of equations. Further detailed numerical procedure of MDFEM and our specific development for Tersoff potentials are available in our previous work [29] and references therein. Initial positions of atoms are generated by using the B-N bond length of 1.444 Å taken from previous MD simulations [30] at optimized structure at 0 K with the same force field. (5, 5) BN armchair and (9, 0) BN zigzag tubes are considered. Difference in diameters of these two tubes is less than 4%. The diameter is about 0.717 and 0.689 nm for (9, 0) BN armchair and (5, 0) BN zigzag tubes, respectively.

3 Results and Discussion

Figure 2 shows the variations of the bending moment versus the bending angle of (9, 0) and (5, 0) BN tubes with the length–diameter ratio $L/D = 30$. The bending angle θ is here defined as the angle between two planes containing the two ends of the tube under bending. It can be seen from Fig. 2 that the bending moment increases monotonously with an increase of the bending angle up to a critical value, and then the bending moment drops suddenly, demonstrating a brittle fracture. The critical bending angle of the (9, 0) BN zigzag tube is approximately 66.6°, 136.6°, 210.6°, and 278.0° for $L/D = 10, 20, 30,$ and $39,$ respectively. The critical bending angle of the (5, 5) BN armchair tube is about approximately 121.7°, 142.9°, 176.7°, and 181.0° for $L/D = 10, 20, 30,$ and $40,$ respectively.

Figure 3 shows the effects of tube's length on the variations of the critical bending moments, critical bending angle, and critical bending curvature of these

Fig. 2 Variations of the bending moment versus the bending angle of the (9, 0) and (5, 0) BN tubes with $L = 30D$

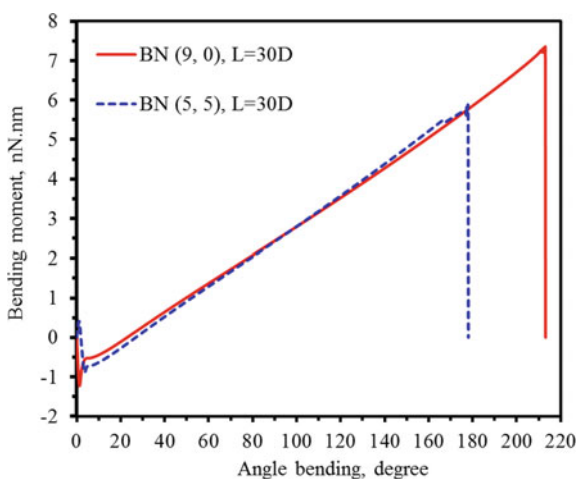
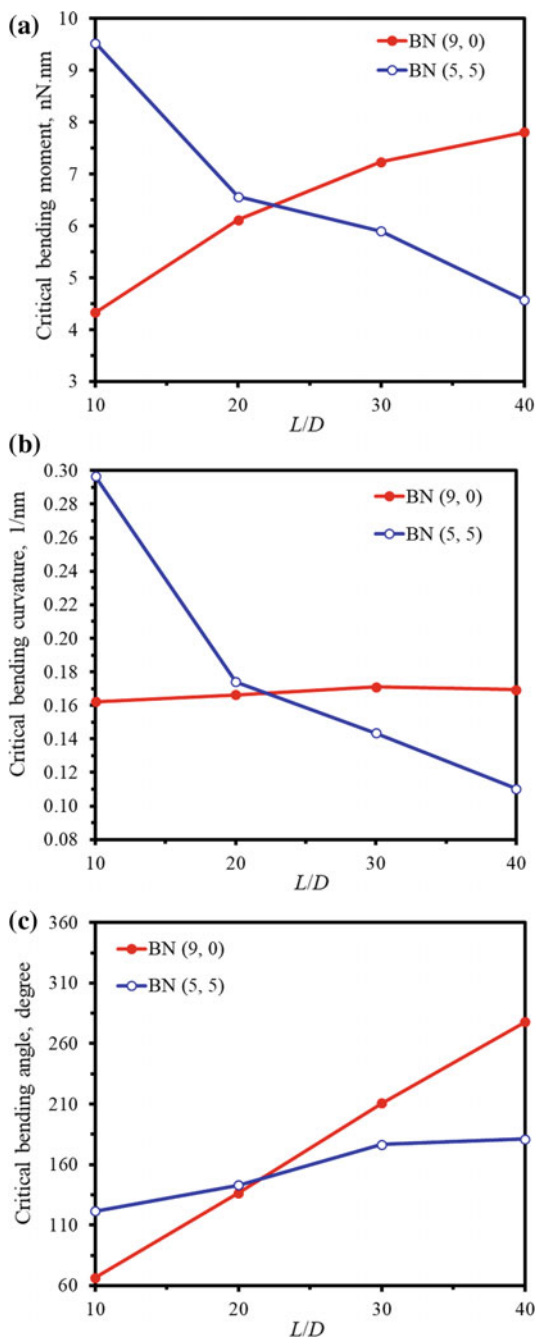


Fig. 3 Variations versus the tube length of: **a** the critical bending angle; **b** critical bending curvature; and **c** critical bending moment



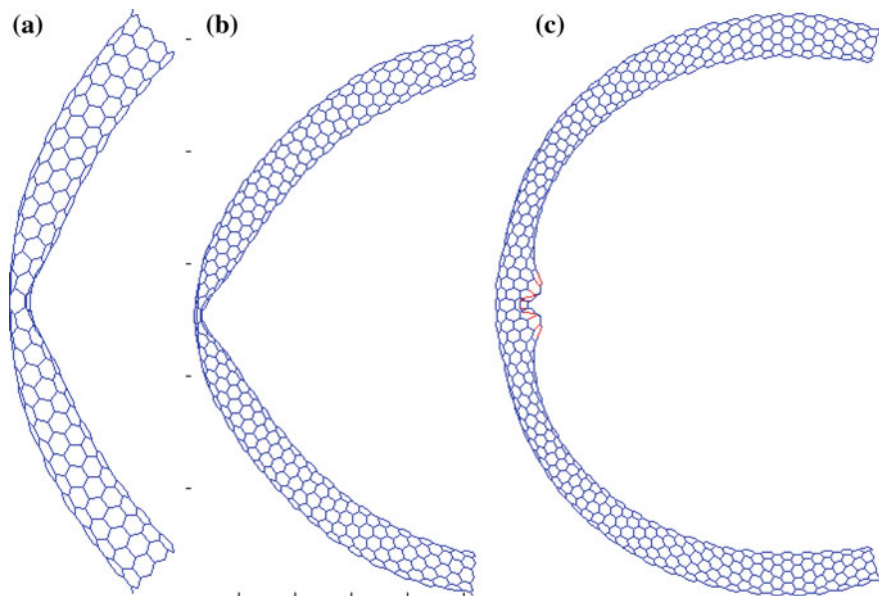


Fig. 4 Post-buckling shapes of (9, 0) BN zigzag tubes: **a** $L/D = 10$, $\theta = 91.67^\circ$; **b** $L/D = 20$, $\theta = 171.89^\circ$; and **c** $L/D = 30$, $\theta = 213.37^\circ$

two tubes. The critical bending moment and the critical bending curvature of (9, 0) BN tubes increase with an increase of the tube's length in the range $L/D = 10$ –40, whereas the critical bending moment and the critical bending curvature decrease when increasing the length of the (5, 5) BN tube. The critical bending angles of these two tubes increase with increasing the tube's length.

The critical bending moment, the critical bending curvature, and critical bending angle of (5, 5) tubes are higher than those of (9, 0) tubes when $L/D = 10$, hence short (5, 5) tubes resist better than short (9, 0) tubes under bending. Whereas long (9, 0) tubes undergo bending better than long (5, 5) tubes; the critical bending moment, the critical bending curvature, and critical bending angle of (9, 0) tubes are higher than those of (5, 5) tubes at $L/D = 30$ and 40 as indicated in Fig. 3. Figure 4 shows the post-buckling shapes of (9, 0) BN zigzag tubes with $L/D = 10$, 20, and 30. Snapshots under progressive bending are depicted in Figs. 5 and 6 for (9, 0) BN zigzag tube with $L/D = 39$ and (5, 5) BN armchair tube with $L/D = 20$, respectively.

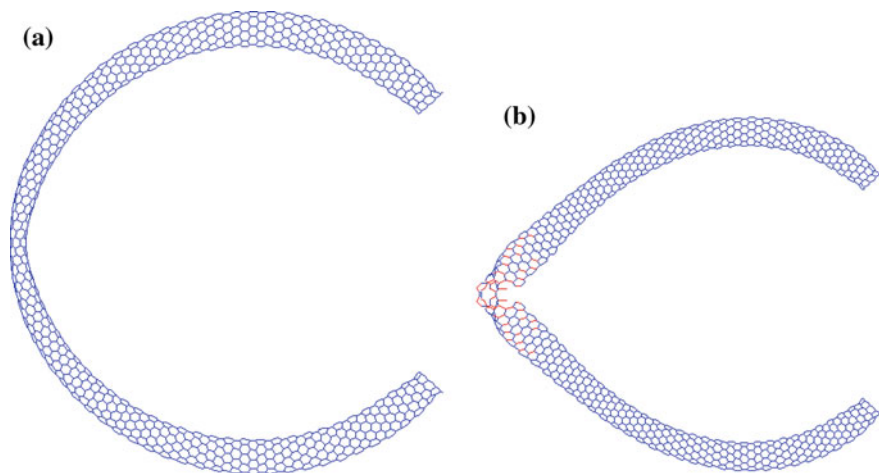


Fig. 5 Snapshots of a (9, 0) BN zigzag tube with $L/D = 39$ under a bending angle of: **a** 279.37°; and **b** 279.49°

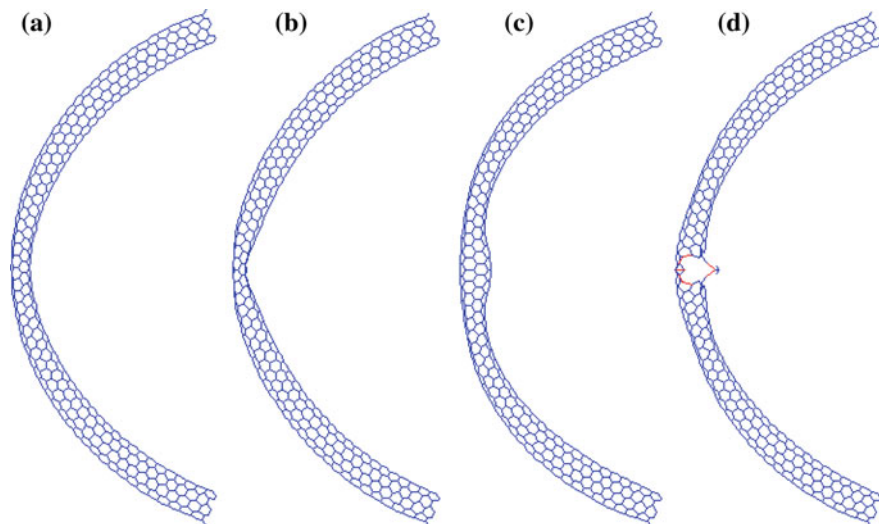


Fig. 6 Snapshots of a (5, 5) BN armchair tube with $L/D = 20$ under a bending angle of: **a** 143.35°; **b** 143.58°; **c** 143.70°; and **d** 143.81°

4 Conclusions

We present the simulation results of the buckling behavior of BN nanotubes under bending with the use of MDFEM. We have found that the tube length affects significantly the bending behavior of the tube. All tubes exhibit brittle fracture under bending. The buckling takes place in the middle of the compressive side of the tube. More investigation should be done to analyze in details the buckling behavior of the BN tubes.

Acknowledgements Danh-Truong Nguyen's work was funded by Vietnam National Foundation for Science and Technology Development (NAFOSTED) under grant number 107.02-2016.13.

References

1. Iijima S (1991) Helical microtubules of graphitic carbon. *Nature* 354(6348):56
2. Zhi C, Bando Y, Tang C, Golberg D (2010) Boron nitride nanotubes. *Mater Sci Eng R Rep* 70(3):92–111
3. Arenal R, Wang M-S, Xu Z, Loiseau A, Golberg D (2011) Young modulus, mechanical and electrical properties of isolated individual and bundled single-walled boron nitride nanotubes. *Nanotechnology* 22(26):265704
4. Chen Y, Zou J, Campbell SJ, Le Caer G (2004) Boron nitride nanotubes: pronounced resistance to oxidation. *Appl Phys Lett* 84(13):2430–2432
5. Baumeier B, Krüger P, Pollmann J (2007) Structural, elastic, and electronic properties of SiC, BN, and BeO nanotubes. *Phys Rev B* 76(8):085407
6. Guo G, Ishibashi S, Tamura T, Terakura K (2007) Static dielectric response and Born effective charge of BN nanotubes from ab initio finite electric field calculations. *Phys Rev B* 75(24):245403
7. Chang C, Fennimore A, Afanasiev A, Okawa D, Ikuno T, Garcia H, Li D, Majumdar A, Zettl A (2006) Isotope effect on the thermal conductivity of boron nitride nanotubes. *Phys Rev Lett* 97(8):085901
8. Attacalite C, Wirtz L, Marini A, Rubio A (2013) Efficient Gate-tunable light-emitting device made of defective boron nitride nanotubes: from ultraviolet to the visible. *Sci Rep* 3
9. Li LH, Chen Y, Lin M-Y, Glushenkov AM, Cheng B-M, Yu J (2010) Single deep ultraviolet light emission from boron nitride nanotube film. *Appl Phys Lett* 97(14):141104
10. Meng W, Huang Y, Fu Y, Wang Z, Zhi C (2014) Polymer composites of boron nitride nanotubes and nanosheets. *J Mater Chem C* 2(47):10049–10061
11. Nautiyal P, Gupta A, Seal S, Boesl B, Agarwal A (2017) Reactive wetting and filling of boron nitride nanotubes by molten aluminum during equilibrium solidification. *Acta Mater* 126:124–131
12. Kang JH, Sauti G, Park C, Yamakov VI, Wise KE, Lowther SE, Fay CC, Thibeault SA, Bryant RG (2015) Multifunctional electroactive nanocomposites based on piezoelectric boron nitride nanotubes. *ACS Nano* 9(12):11942–11950
13. Chandra A, Patra PK, Bhattacharya B (2016) Thermomechanical buckling of boron nitride nanotubes using molecular dynamics. *Mater Res Express* 3(2):025005
14. Huang Y, Lin J, Zou J, Wang M-S, Faerstein K, Tang C, Bando Y, Golberg D (2013) Thin boron nitride nanotubes with exceptionally high strength and toughness. *Nanoscale* 5(11):4840–4846

15. Li T, Tang Z, Huang Z, Yu J (2017) A comparison between the mechanical and thermal properties of single-walled carbon nanotubes and boron nitride nanotubes. *Physica E* 85:137–142
16. Kinoshita Y, Ohno N (2010) Electronic structures of boron nitride nanotubes subjected to tension, torsion, and flattening: a first-principles DFT study. *Phys Rev B* 82(8):085433
17. Anoop Krishnan N, Ghosh D (2014) Defect induced plasticity and failure mechanism of boron nitride nanotubes under tension. *J Appl Phys* 116(4):044313
18. Anoop Krishnan N, Ghosh D (2014) Chirality dependent elastic properties of single-walled boron nitride nanotubes under uniaxial and torsional loading. *J Appl Phys* 115(6):064303
19. Xiong Q-L, Tian XG (2015) Torsional properties of hexagonal boron nitride nanotubes, carbon nanotubes and their hybrid structures: a molecular dynamics study. *AIP Adv* 5(10):107215
20. Garel J, Leven I, Zhi C, Nagapriya K, Popovitz-Biro R, Golberg D, Bando Y, Hod O, Joselevich E (2012) Ultrahigh torsional stiffness and strength of boron nitride nanotubes. *Nano Lett* 12(12):6347–6352
21. Tanur AE, Wang J, Reddy AL, Lamont DN, Yap YK, Walker GC (2013) Diameter-dependent bending modulus of individual multiwall boron nitride nanotubes. *J Phys Chem B* 117(16):4618–4625
22. Zhang J (2016) Size-dependent bending modulus of nanotubes induced by the imperfect boundary conditions. *Sci Rep* 6
23. Hollerer S (2014) Numerical validation of a concurrent atomistic-continuum multiscale method and its application to the buckling analysis of carbon nanotubes. *Comput Methods Appl Mech Eng* 270:220–246
24. Wang C, Liu Y, Al-Ghalith J, Dumitrică T, Wadee MK, Tan H (2016) Buckling behavior of carbon nanotubes under bending: from ripple to kink. *Carbon* 102:224–235
25. Tersoff J (1989) Modeling solid-state chemistry: Interatomic potentials for multicomponent systems. *Phys Rev B* 39(8):5566
26. Sevik C, Kinaci A, Haskins JB, Çağın T (2011) Characterization of thermal transport in low-dimensional boron nitride nanostructures. *Phys Rev B* 84(8):085409
27. Liu B, Huang Y, Jiang H, Qu S, Hwang KC (2004) The atomic-scale finite element method. *Comput Methods Appl Mech Eng* 193:1849–1864
28. Wackerfuß J (2009) Molecular mechanics in the context of the finite element method. *Int J Numer Meth Eng* 77:969–997
29. Le MQ, Nguyen DT (2014) Atomistic simulations of pristine and defective hexagonal BN and SiC sheets under uniaxial tension. *Mater Sci Eng, A* 615(2014):481–488
30. Le M-Q (2014) Atomistic study on the tensile properties of hexagonal AlN, BN, GaN, InN and SiC sheets. *J Comput Theor Nanosci* 11(6):1458–1464